Construction and Building Materials 320 (2022) 126206

Contents lists available at ScienceDirect

Construction and Building Materials

journal homepage: www.elsevier.com/locate/conbuildmat

Quantification of the cement paste and phase's association in fine recycled aggregates by SEM-based image analysis

Carina Ulsen *, Renato Contessotto, Rafael dos Santos Macedo, Henrique Kahn

Universidade de São Paulo - Technological Characterization Laboratory - Escola Politécnica – Department of Mining and Petroleum Engineering, Brazil

ARTICLE INFO

Keywords:
SEM-based image analysis
Construction and demolition waste
Recycled fine aggregates
recycled sand

ABSTRACT

Fine recycled aggregates represent a substantial amount of total recycled aggregates generated in the construction and demolition waste recycling process, nevertheless its use is limited, and characterization procedures are not well established. The liberation of cement paste and the understanding of the mineral phase's composition and association is essential to improve fine recycled aggregates quality and to drive recycling process. This study carried out extensively X-ray SEM-based image analysis to quantify cement paste and other phases to evaluate associations and liberation of each phase. The results show that >80% in mass are composed mostly by natural aggregates. Considering just higher densities (d >2.60 g/cm^3), almost all particles are free from cement paste (96% in mass). The correlations achieved between the chemical analysis and mineral composition demonstrated the reliability of automated image analysis as characterization tool for fine recycled aggregates.

1. Introduction

The quantification of cement paste in recycled aggregates (RA) is pursued by the academic community. The cement paste quantification is essential to evaluate the effectivity of recycling process in cement based recycled aggregates. Achieving the cement paste and mineral phases associations and contents, it is possible to develop a hierarchically process design according with the properties of the construction and demolition wastes (CDW). Process control is the key to improve the recycled aggregate quality. Therefore, the enhancement of recycled aggregates applications will be inherent to the process, contributing to favour circular economy. [1,2] The correct selection of crusher clearly influences the final product. The devices commonly used in mineral processing industry, as jaw and impact crushers, vertical shaft impactors, ball mill, have proved to be efficient in remove partially cement paste [4–7].

The CDW processing also contributes to improve the recycled aggregates quality. Seeking new technologies to discretize phases is equal in importance of pursuit the critical driven force to concentrate mineral phases. The increase in the processing cost is a considerable barrier to practical application. In contrast, the decreases in natural resources extraction and the high amount of construction waste currently generated in volume positively boost new technologies.

The cement paste (CP) porosity is the major cause for lessening the mechanical properties of recycled concrete aggregates, such as compression resistance, Los Angeles abrasion, low density and high-water absorption [3]. The quantification of cement paste is obtained by simple methods with considerable drawbacks. Acid leaching method overestimates the cement paste content when recycled aggregates contain some limestone [8]; X-ray fluorescence could be employed by the sum of calcium oxide content (CaO) and loss of ignition (LOI) to estimate the percentage of cement paste plus carbonate contents [9]. New simple methods have been developed in the literature, but these innovative methods [10,11] were not tested enough to ensure reliability considering recycled aggregates heterogeneity. At best of our knowledge, no reported method quantifies cement paste and all mineral phases present considering fine recycled aggregate.

In mineral processing, it is important to identity and quantify the presence of each phase and its association, once a selected driven force is employed for phase's separation (e.g. density and magnetic susceptibility) to split the desire or undesired phases. Therefore, measuring modal mineralogy [12,13] and CP content and its associations is fundamental to elucidate which would be the best set of recycling mineral processing parameters [4–7,15] in each processing step: comminution, classification and separation, for improve final product quality (reduced CP and therefore, porosity).

Mineral associations are traditionally carried out by mineral separations in laboratory scale, taking into account the differences in the

* Corresponding author at: Department of Mining and Petroleum Engineering, Polytechnic School, University of Sao Paulo, Av. Prof. Mello Moraes, 2373, Butantã, São Paulo, SP CEP 05508-030, Brazil.
E-mail address: carina.ulsen@usp.br (C. Ulsen).

https://doi.org/10.1016/j.conbuildmat.2021.126206
Received 10 September 2021; Received in revised form 15 December 2021; Accepted 22 December 2021
Available online 25 January 2022

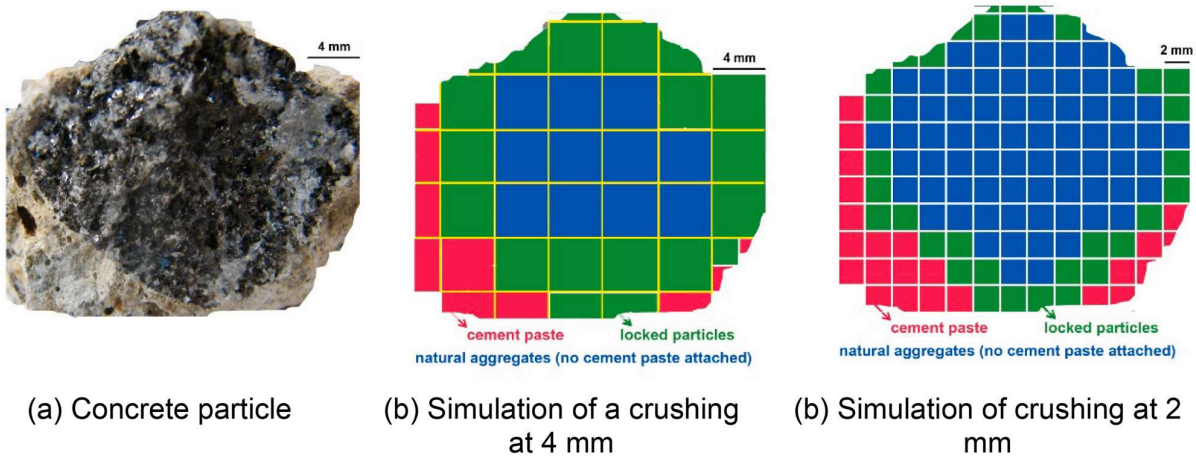

Fig. 1. Schematic representation of the liberation degree for a crushing lattice [7]. "Reprinted figure from "Concrete aggregates properties crushed by jaw and impact secondary crushing", Volume 8, Issue 1, January–March 2019, with permission from Elsevier." License number 5210280802844.

physical properties of phases, such as density and magnetic susceptibility [14–18]. In the 90s, phases association starts to be evaluated by image analysis, such as optical microscopy or scanning electron microscopy (SEM) [17,19]. The origin of phase identification and quantification by SEM, starts with identifications of grey level of backscattered-electron images for each mineral stablishing individual thresholds. The technological evolution improved the linear and areal statistical analysis for high resolution and high contrast images. At 2003, Gu [20] presented the mineral liberation analysis (MLA) as SEM-automated tool, representing a method that combines de bbackscattered-electron (BSE) images analysis and energy dispersive X-ray spectroscopy (EDS). This combination permits unequivocally associate the grey level with the chemical signature of each phase improving the histogram thresholds and quantifications of the phases automatically

The phase's quantification by image analysis is poorly described in the literature for RA characterization; its objectives essentially the cement paste quantification. Abbas, et al (2009) [21] described the procedure of image analysis for polished concrete species (400x100x100 mm) produced by coarse recycled concrete aggregates (4.75 to 19.0 mm) and image acquisition by a photographic camera; phases identification was based on the colour of phases correlated to limestone natural aggregates [21]. The authors evaluated aggregates particles in coarse faction, therefore, a large number of particles are needed to ensure good representativeness of the sample; even with automated image analysis, it is not a simple task to ensure the accuracy of the results, since polished sections will fit not more than a dozen particles.

The applications of image analysis techniques in multi-scale characterization are described by the study of Pradhan, Kumar and Barai (2020) aiming to evaluate unhydrated cement phases and void contents, correlating it with concrete hardness and compressive strength [22]. The interface transitional zone (ITZ) is also explored for recycled aggregates by image analysis; Zhao et al; 2015 [23] studied the association of old mortar and new mortar in fine recycled aggregates by BSE images associated with EDS analysis to reveal its impacts in compressive strength. Kim, Y. et. al. (2019) [24] reported by the first time in literature, pore segmentation by BSE image analysis for porosity assessment and cement paste content for recycled concrete aggregates (RCA).

Fine recycled aggregates (FRA; <5 mm, filler and sand fraction) represent 40 to 60% of the total recycled aggregate, in mass. The FRA fraction is almost disregarded in the recycling process. The literature shows that almost all the cement paste content is concentrated in fine fraction (<5 mm) after crushing process [25].

The efficiency of CDW recycling process is related mainly with the cement paste content, meanwhile the liberation and association of mineral phases (quartz, feldspar, carbonates and other) have equivalent importance. The SEM-based automated image analysis (SEM-IA) represent an alternative to drive recycling process and evaluates the phase's content, association and liberation in a single analysis for FRA.

This paper aims to appraise the composition of fine recycled aggregates by SEM-based image analysis (SEM-IA), phase's association and their liberation to drive recycling process, especially the comminution mesh. Moreover, the partition (distribution) of elements of interest on bearing particles was determined.

1.1. *Definitions*

Some definitions used in this work are important to be addressed for a better understanding of the experimental data and results.

Image analysis and stereology – image analysis is widely used in minerals characterization to identify and quantify phases occurrence and associations; it concerns the measurement of geometrical features that are exposed on two-dimensional images. The images acquisition is commonly carried out from plane sections cut through mounted minerals particles [18]. Image acquisition can be done by different microscope techniques, from optical to electron microscopes. Nevertheless, in order to obtain representative image analysis considering three-dimensional information, particles must be randomly distributed.

The correlation of measured data on degraded space dimensionality is a field of science called "stereology" [26]. The principle of stereology states that the volumetric proportion (3D information) of each phase is equivalent to its area or line proportion (2D or 1D data) if sufficient particles are analyzed (statistically representative) in a random section (or sections) of the sample [18,26]. The first record of quantitative mineralogical composition by image analyzing was in 1848 with the studies of De Lesse; different image acquisition and processing systems have been optimized over the years, but De Lesse principle remain applicable [27].

Liberation – in mineral processing, degree of liberation of a certain phase is represented by percentage of the phase occurring in free particles (single phase particle) in relation to the total of that phase in the material (free + locked/composite particles) [28]. Liberation occurs when dissimilar phases, such as hardened cement paste and natural aggregates phases, are detached from each other. Liberation is mainly achieved by size reduction; therefore, crushing is the first necessary step release of usable materials from concrete waste, including gravel, crushed aggregates and sand. In Fig. 1, it can be seen an image of a concrete particle (Fig. 1a and the liberation achieve by crushing at 4 mm (Fig. 1b and 2 mm (Fig. 1c demonstrating the finer the comminution, the higher the degree of liberation, i.e., the finer the comminution, more particles free from the cement paste are produced. In this example, the

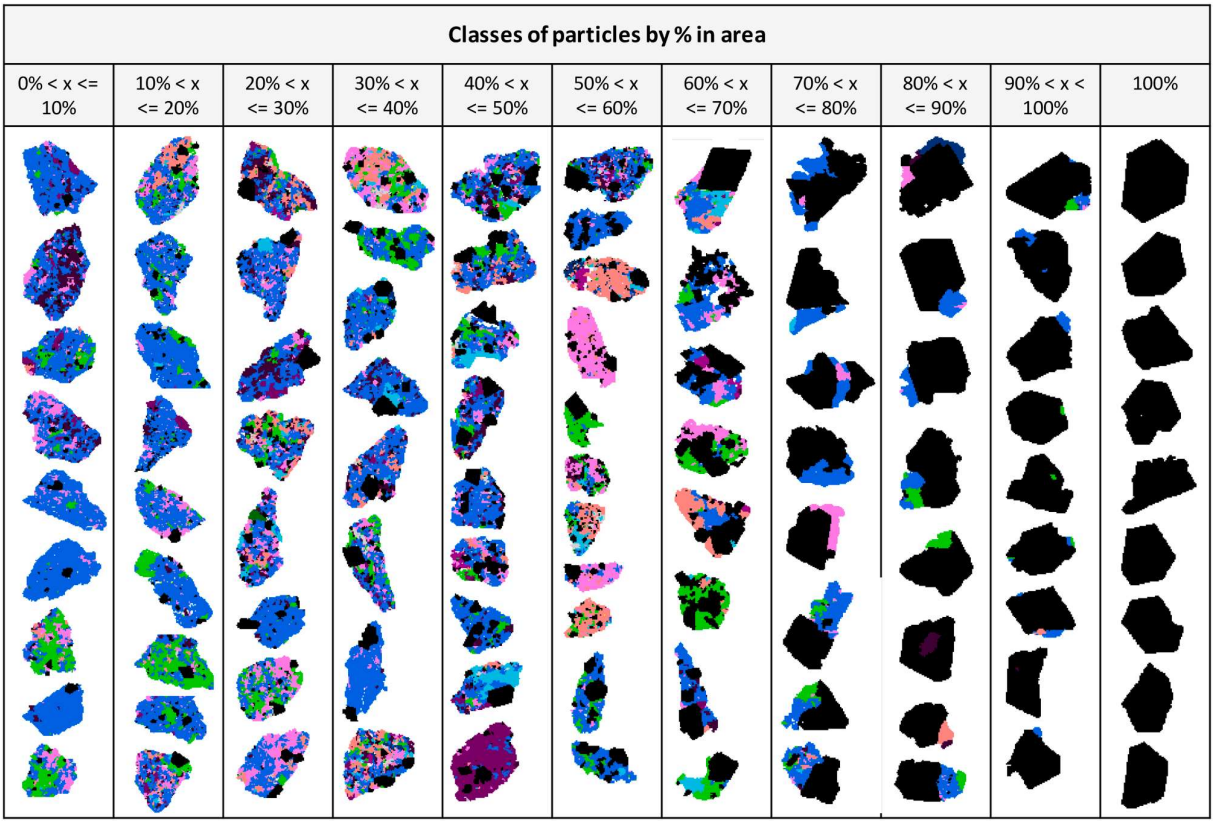

Fig. 2. Schematic representation of the classes of particles by percentage in area (phase of interest in black).

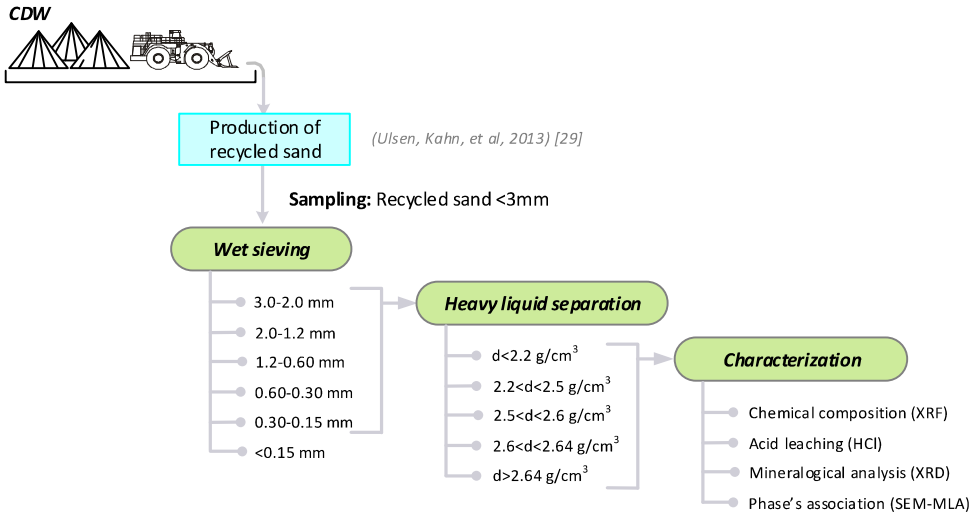

Fig. 3. Flowchart of sample preparation for SEM-based automated image analysis.

reduction of the top size from 4 to 2 mm, led to an increasing of liberation degree. An example to make clear the calculations of liberation degree is shown in Fig. 11 in Appendix I.

Liberation curves – liberation degree can be indicated by a number when considering the whole sample as well as by fraction size or liberation class. Each class indicate the percentage of a certain phase in the particle. In Fig. 2 it is illustrated different classes of particles containing from 0% to 100% of a certain phase (in this case indicated in black color). Therefore a "liberation curve" can be traced and indicates the cumulative frequency of the phase of interest that occurs for each particle class.

2. Materials and methods

2.1. Samples

This study was performed on fine recycled aggregates obtained by tertiary crushing of approximately 4 tons of CDW by a vertical shaft impactor (VSI) to below 3 mm (classified as fine recycled aggregate or

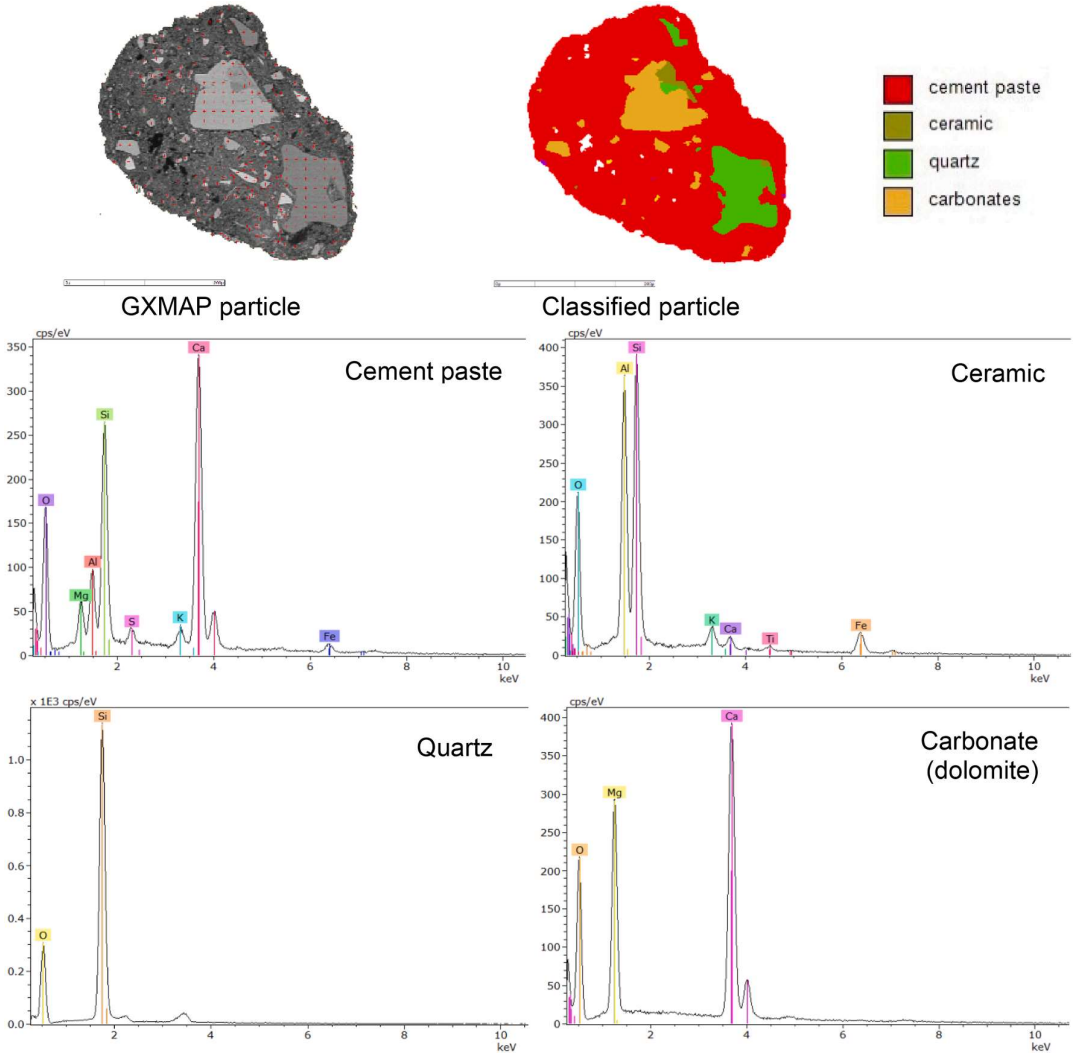

Fig. 4. Phase discrimination by BSE gray level and EDS spectra at GXMAP mode.

sand).

The processing of CDW focused on the production of recycled fine aggregates lead to a better quality of products [29,30]. When recycling is targeted to the production of coarse recycled aggregates, sand fraction is involuntarily generated as a by-product (in a few cases), but mostly as tailing and its composition is mostly fragile particle edges that broke off during handling or demolition as well as in the grinding processes [30]. Additionally, the use of vertical shaft impactors (VSI) proved to improve the roundness and sphericity of the particles, contributing to a better aggregate morphology, for manufactured sand [31,32] and recycled aggregates [29,30] with some operational advantages as control of the particle size distribution by rotor rotation [32], low labour costs, no crushing of the fines, and lower energy consumption compared to cone crushers (6% less energy) for the same feed rate [33].

The sampling procedure (60 days of sampling) and crushing (primary, secondary and tertiary crushing) was described previously in literature [29]. Sampling of CDW was carried out in a private recycling plant located in Sao Paulo metropolitan region (large metropolitan area in Brazil) which composition is mostly low and medium-strength concrete (around 80%) and masonry. The recycled sand (VSI-75) obtained was homogenized and sampled in order to guarantee representative aliquots for this study. The characterization by automated image system (SEM coupled with MLA – Mineral Liberation Analyser) was performed on polished sections of selected samples sub-categorized by sieve fractions and specific gravity ("d") (Fig. 3).

The sample preparation study comprised wet sieving in fractions for a better sample preparation and characterization (down to 0.15 mm) (Haver&Bocker EML45 equipment) and specific gravity separations in heavy liquid (bromoform admixtures with ethylic alcohol) at specific densities ("d") of 2.20, 2.50, 2.60 and 2.64 g/cm^3 for minerals separation. After that each product was sampled in a rotary sampler to assure sample representativeness. Each product was pulverized for chemical analysis. Images from stereomicroscope from a selected size fraction of the attained products from density separation are shown in Fig. 15, in Appendix III.

2.2. Chemical Analysis: X-ray fluorescence and acid leaching

The chemical quantitative analysis of all products was performed by X-ray fluorescence spectrometry (XRF) in Axios Advance equipment (Malvern Panalytical) using fused beads with anhydrous lithium tetraborate according to the analytical laboratory quality control procedures, considering the calibration curves established from certified reference materials. The loss on ignition (LOI) was obtained by thermal treatment in muffle at 1050 °C for one hour.

The estimation of the content of cement paste plus carbonates was

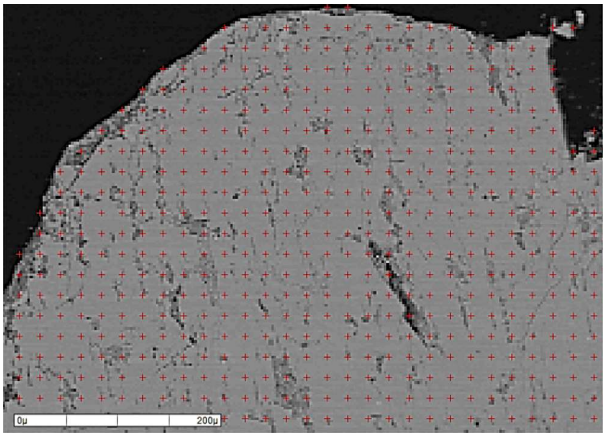

Fig. 5. Phase classification of particles in by EDS mapping. Each red cross represents an EDS data acquired.

Table 1
Strategies of segmentation for the main phases.

Phase	Composition	discrimination criteria	discrimination difficulty
Cement paste	Highly variable	BSE + EDS map + further manual image processing (touch up)	Similar BSE gray level of ceramic, feldspar and carbonates. Minor components of quartz from cement paste matrix can be classified as quartz instead of cement paste; solved by touch up
Ceramic	Highly variable	BSE + EDS map + further image processing (touch up)	Similar BSE gray level of cement paste, feldspar and carbonates. Minor components of feldspar into ceramic matrix can be classified as feldspar instead of ceramic; solved by touch up
Feldspar	Variable	BSE + EDS map	Similar BSE gray level of cement paste, ceramic and carbonates; solved by BSE + EDS
Carbonate	Variable	BSE + EDS map	Similar BSE gray level of cement paste, ceramic and feldspar; solved by BSE + EDS
Phyllosilicates	Variable	BSE + EDS map	Normal composition variations between those in the family, such as higher/lower presence of K or Mg depends on phyllosilicates types but easy to solve with EDS
Pyroxene/ amphibole	little variable	BSE + EDS point	–
Quartz	Fixed	BSE + EDS point	–
Anatase	Fixed	BSE + EDS point	–

carried out by acid leaching with a 33% HCl solution on pulverized samples [34].

2.3. SEM-based automated image analysis (SEM-IA)

The assessment of the composition of the phase associations in the products was carried out by automated image analysis system (MLA – Mineral Liberation Analyser) coupled to a SEM (Quanta 600 FEG – FEI/ THERMO) assisted by energy-dispersive X-ray spectroscopy (EDS) (Quantax 4030, Bruker). A brief description about how the SEM-IA works is shown in Appendix II. Minerals identification was supported by X-ray diffraction analysis in pulverized samples and backload pressing.

The preparation of monolayer polished sections for image analysis was carried out by size fraction and density products and considered multiples sections to assure reproducibility and to achieve the statistical representativeness, where: 0.30–0.15 mm: 5 sections, 0.60–0.30 mm and 1.2–0.60 mm – 10 section each fraction, 2.0–1.2 mm and >2.0 mm – 14 sections each fraction. At the total, >56,000 particles were analysed. Increasing the number of particles analysed, there is a decrease the deviation as postulated by Van der Plas in 1965; according to the chart they developed, counting 3,000 points/grains would lead to <2% on absolute standard deviation [35]. Additionally, using the calculations they presented, a relative deviation of 10% would require counting 4000 points/grains for phases content of 10%, 600 points/grains for phases content of 40% and 200 points/grains for phases occurrence of 70%. In summary, the authors postulate that reliability is expressed by standard deviation that is related to the number of points counted of each phase.

Sampling of all products was carried out in a rotatory sample divider MSR25 Microscal considering from 60 to 80 incremental aliquots to assure representative aliquots for further microscope analysis. The monolayer polished sections were prepared spreading the particles homogeneously in a cylindrical mold and filled with epoxy resin; the blocks were demolded after hardening and followed by grinding and polishing steps.

The monolayer polished sections, previously covered with carbon film, were submitted to the SEM-based image analysis routine in GXMAP mode at MLA system [17] (Fig. 4) from which classification of the phases was obtained in a first step by backscattered electron imaging (BSE) and gray levels segmentation (atomic number contrast) and further by chemical differentiation through a net of EDS point analysis (characteristic X-ray spectra). In this procedure, specific gray level ranges with two or more phases having a similar atomic number (BSE contrast) can be chemically discriminated throughout a more detailed EDS analysis in a regular net with a desirable pixel size, for example, ceramics and carbonates. In Fig. 12 (Appendix II) it is also show the phase's discrimination of very complex texture particles.

2.4. Phase discrimination strategy

The cement paste, ceramic, feldspar and carbonates sometimes have similar grey level. It happens because BSE levels reflects the average atomic weight; the composition of those phases varies a lot and it can produce similar grey levels. Therefore, phase's discrimination was solved by applying a segmentation based on the X-ray EDS profile – so called GXMAP mode. The distances of each X-ray mapping as illustrated in Fig. 5. By using this approach, small grains of quartz in the matrix of cement paste could be classified as a quartz, nevertheless, the texture was considered essential to differentiate these particles and the "touch up" tool was applied to correct occasional misunderstanding classification. The same happen with ceramic phase, in this case the phase was misunderstood as feldspar. Table 1 summarizes the segmentation strategy applied for the main phases.

3. Results and discussions

3.1. Products phase composition

Products composition by size and density is shown in Table 2, as well as phase's distribution. The summary of composition by size fraction and density is shown in Appendix III (Fig. 13 and Fig. 14), as well as images from stereomicroscope from a selected size fraction (Fig. 15). Images from classified particles from SEM-IA by size and density is shown in

Table 2
Content and distribution of mineral phases by size fraction and density.

	Fraction (mm)/ Products (g/cm³)	% weight assay	Content by SEM-IA (%)								Distribution by SEM-IA (%)							
			qz	fd	cp	carb	cer	mic	ma	oth	qz	fd	cp	carb	cer	mic	ma	Oth
3.0-2.0 mm	d<2.2	6.2	57	5.7	30	2.7	3.9	1.2	0.0	0.3	10.1	1.0	23.5	2.9	5.1	1.2	0.0	1.8
	2.2<d<2.5	24.0	52	21	16	4.8	4.3	0.8	0.0	0.4	35.7	14.3	49.9	20.6	22.0	3.3	0.0	8.1
	2.5<d<2.6	17.0	27	43	8.1	4.3	14	2.0	0.3	0.4	13.1	20.6	17.6	13.1	52.0	5.8	1.2	6.4
	2.60<d<2.64	12.0	43	42	1.9	3.1	1.0	6.1	1.7	0.9	14.8	14.1	2.9	6.7	2.5	12.1	5.4	10.1
	d>2.64	40.8	23	44	1.2	7.8	2.1	11	8.8	2.0	26.3	50.1	6.1	56.7	18.3	77.7	93.4	73.6
	Total	**100**	**35**	**36**	**7.8**	**5.6**	**4.7**	**6.0**	**3.9**	**1.1**	**100**	**100**	**100**	**100**	**100**	**100**	**100**	**100**
2.0-1.2 mm	d<2.2	6.7	46	6.1	39	3.3	3.6	1.1	0.0	0.4	6.7	1.4	30.2	5.1	5.8	1.7	0.0	2.4
	2.2<d<2.5	25.0	57	17	18	2.9	4.1	1.0	0.0	0.3	30.8	14.6	50.5	16.9	24.5	5.3	0.1	7.7
	2.5<d<2.6	18.7	39	43	4.5	1.0	9.7	1.1	1.1	0.4	15.5	28.2	9.7	4.4	44.1	4.5	10.4	7.0
	2.60<d<2.64	20.5	62	31	1.6	0.2	2.3	2.3	1.1	0.3	27.0	21.8	3.8	0.9	11.6	10.5	11.2	6.3
	d>2.64	29.2	32	34	1.7	10.7	2.0	12.2	5.2	2.7	20.0	34.0	5.7	72.7	14.1	78.1	78.3	76.6
	Total	**100**	**47**	**29**	**8.7**	**4.3**	**4.1**	**4.5**	**1.9**	**1.0**	**100**	**100**	**100**	**100**	**100**	**100**	**100**	**100**
1.2-0.60 mm	d<2.2	4.8	36	5.5	51	2.5	3.6	0.8	0.0	0.5	3.1	1.2	27.1	3.9	5.0	1.3	0.0	2.6
	2.2<d<2.5	22.2	47	19	22	2.5	6.7	1.2	0.0	1.0	18.7	18.7	54.9	18.1	43.8	9.0	0.0	23.5
	2.5<d<2.6	19.9	54	35	4.7	0.8	4.1	0.6	0.0	0.2	19.2	31.1	10.4	5.3	24.2	4.2	0.0	4.5
	2.60<d<2.64	28.3	79	17	1.2	0.3	0.8	0.7	0.6	0.1	39.9	21.4	3.8	3.0	6.8	6.3	8.7	3.4
	d>2.64	24.8	43	25	1.4	8.7	2.8	9.6	6.6	2.5	19.1	27.6	3.8	69.7	20.2	79.1	91.3	66.0
	Total	**100**	**56**	**22**	**9.1**	**3.1**	**3.4**	**3.0**	**1.8**	**0.9**	**100**	**100**	**100**	**100**	**100**	**100**	**100**	**100**
0.60-0.30 mm	d<2.2	4.8	16	5.6	71	1.8	3.3	0.8	0.4	0.5	1.2	1.7	34.0	3.6	6.4	1.7	1.0	2.7
	2.2<d<2.5	15.6	48	17	27	2.3	3.4	1.6	0.8	0.6	11.7	16.6	41.3	14.9	21.6	11.0	5.8	9.6
	2.5<d<2.6	17.6	49	37	7.7	1.0	3.8	0.6	0.7	0.2	13.4	41.5	13.5	7.1	27.6	4.9	5.8	3.7
	2.60<d<2.64	45.1	88	7.6	1.8	0.2	1.3	0.3	0.5	0.1	61.8	21.9	8.2	4.4	24.8	6.5	11.1	4.5
	d>2.64	16.9	45	17	1.8	9.7	2.8	10.2	9.2	4.3	11.8	18.2	3.0	69.9	19.6	75.9	76.4	79.6
	Total	**100**	**64**	**16**	**10**	**2.4**	**2.4**	**2.3**	**2.0**	**0.9**	**100**	**100**	**100**	**100**	**100**	**100**	**100**	**100**
0.30-0.15 mm	d<2.2	6.7	9.4	3.9	81	2.3	2.7	0.7	0.0	0.3	1.1	1.8	35.3	6.2	6.5	2.2	0.0	1.4
	2.2<d<2.5	12.2	25	14	49	3.6	5.7	1.7	0.0	0.5	5.2	11.9	39.2	17.3	25.2	9.2	0.0	4.7
	2.5<d<2.6	29.2	59	26	10	1.1	3.2	0.7	0.0	0.1	28.8	53.3	18.3	13.1	34.5	9.3	0.7	3.0
	2.60<d<2.64	34.3	87	8.0	2.2	0.5	1.0	0.4	0.9	0.1	49.8	19.1	4.8	6.1	12.4	5.8	19.0	2.8
	d>2.64	17.7	51	11	2.1	8.1	3.3	9.4	7.7	6.8	15.2	13.9	2.4	57.3	21.4	73.5	80.3	88.2
	Total	**100**	**60**	**14**	**15**	**2.5**	**2.7**	**2.3**	**1.7**	**1.4**	**100**	**100**	**100**	**100**	**100**	**100**	**100**	**100**
	Products	**%wt**	**qz**	**fd**	**cp**	**carb**	**cer**	**mic**	**ma**	**oth**	**qz**	**fd**	**cp**	**carb**	**cer**	**mic**	**ma**	**oth**
Total 3.0-0.15 mm	**d<2.2**	**5.8**	32	5.3	**55**	**2.5**	3.3	0.9	**0.1**	0.4	3.5	1.3	**31.1**	4.3	5.7	1.5	0.2	2.1
	2.2<d<2.5	**19.6**	48	18	**24**	**3.2**	5.0	1.2	**0.1**	0.6	17.6	15.5	**46.0**	17.9	28.5	6.8	1.1	10.8
	2.5<d<2.6	**20.7**	49	35	7.1	1.4	6.1	0.9	0.3	0.2	18.9	32.0	14.3	8.6	37.0	5.5	3.1	4.7
	2.60<d<2.64	**28.7**	79	15	1.7	0.5	1.2	1.1	0.8	0.2	42.6	19.3	4.8	4.2	10.3	8.9	10.3	5.1
	d>2.64	**25.2**	37	29	1.5	8.9	2.5	10.7	7.4	3.3	17.4	31.9	3.8	65.0	18.6	77.3	85.4	77.3
	Total	**100**	**53**	**23**	**10**	**3.5**	**3.4**	**3.5**	**2.2**	**1.1**	**100**	**100**	**100**	**100**	**100**	**100**	**100**	**100**
	d>2.2	**94.2**	55	24	7.5	3.5	3.4	3.6	2.3	1.1	96.5	98.7	68.9	95.7	94.3	98.5	99.8	97.9
	d>2.5	**74.6**	56	25	3.2	3.6	3.0	4.3	2.9	1.2	78.9	83.2	22.9	77.8	65.8	91.7	98.8	87.1
	d>2.6	**53.9**	59	22	1.6	4.4	1.8	5.6	3.9	1.6	**60.0**	**51.2**	**8.6**	**69.2**	**28.8**	**86.2**	**95.6**	**82.4**
	d>2.64	**25.2**	**37**	**29**	**1.5**	**8.9**	**2.5**	**10.7**	**7.4**	**3.3**	17.4	31.9	3.8	65.0	18.6	77.3	85.4	77.3

Notes: qz-quartz. fd – feldspar. cp – cement paste. carb – carbonates. cer - ceramics. mic – micas. ma – mafic minerals (pyroxene+ amphibole). oth – other minor phases

Distribution means the percentage of each phase that is associated to each product, i.e., from the total quartz (or any phase), the proportion that is recovery in each product. These calculations are relevant when thinking on recycling process and products/phases recovery.

$$Distribution = \frac{\%\ mass\ x\ content\ (for\ each\ product)}{total\ grade\ at\ fraction}$$

Example: $\frac{6.2\ x\ 57}{35}$ *=10.1 (highlighted in the table in brown colour)*

Notes: qz-quartz. fd – feldspar. cp – cement paste. carb – carbonates. cer – ceramics. mic – micas. ma – mafic minerals (pyroxene + amphibole). oth – other minor phases.

Distribution means the percentage of each phase that is associated to each product, i.e., from the total quartz (or any phase), the proportion that is recovery in each product. These calculations are relevant when thinking on recycling process and products/phases recovery.

Distribution $= \frac{\%massxcontent(foreachproduct)}{totalgradeatfraction}$. Example: $\frac{6.2x57}{35} = 10.1$ (highlighted in the table in brown colour).

Fig. 6.

The separability of mineral phases by heavy liquid separation efficiency was previously demonstrated in the literature [6] and it is indicated by the products mass distribution in the heavy products. Regarding the density separation for the product (−3.0 + 0.15 mm – Table 2, highlighted in red colour), about 94.2% of sample mass is concentrated in density above 2.20 g/cm^3 containing 7.5% of cement paste; 74.6% in density above 2.50 g/cm^3 with 3.2% of cement paste; 53.9% in density above 2.60 g/cm^3 and just 1.6% of cement paste. These results demonstrate that the density is a driving force that allows the separation of particles enriched in cement paste, as previously described. In terms of recycling process, the removal of a minor amount of mass on light products increases the final product quality (lower cement paste content).

As concerns the sieve sized products, it is notable that the density is more efficient driven force when compared with particle size regarding to phases distribution (Table 2, Fig. 6). However, some important changes are observed in finer fractions, as expected, the content of cement paste increase (from 7.8 to 15%) as well as the quartz content (from 35 to 60%). Some minerals otherwise decrease the content such as feldspar (from 36 to 14%), carbonates (5.6 to 2.5%) and mafic minerals (from 3.9 to 1.7%).

The mass distribution by size and density, evidence the concentration of heavier products (d >2.64 g/cm^3) in coarse fractions, varying from 40.8 to 17.7% (Table 2, highlighted in blue colour) due to the presence of phases resistant to crushing, especially feldspar and mafic minerals (pyroxene + amphibole). Concerning the distribution of each phase it is outstanding that quartz, feldspar, carbonates and mafic minerals concentrates on heavy products, while ceramics in intermediate products and cement paste in light products.

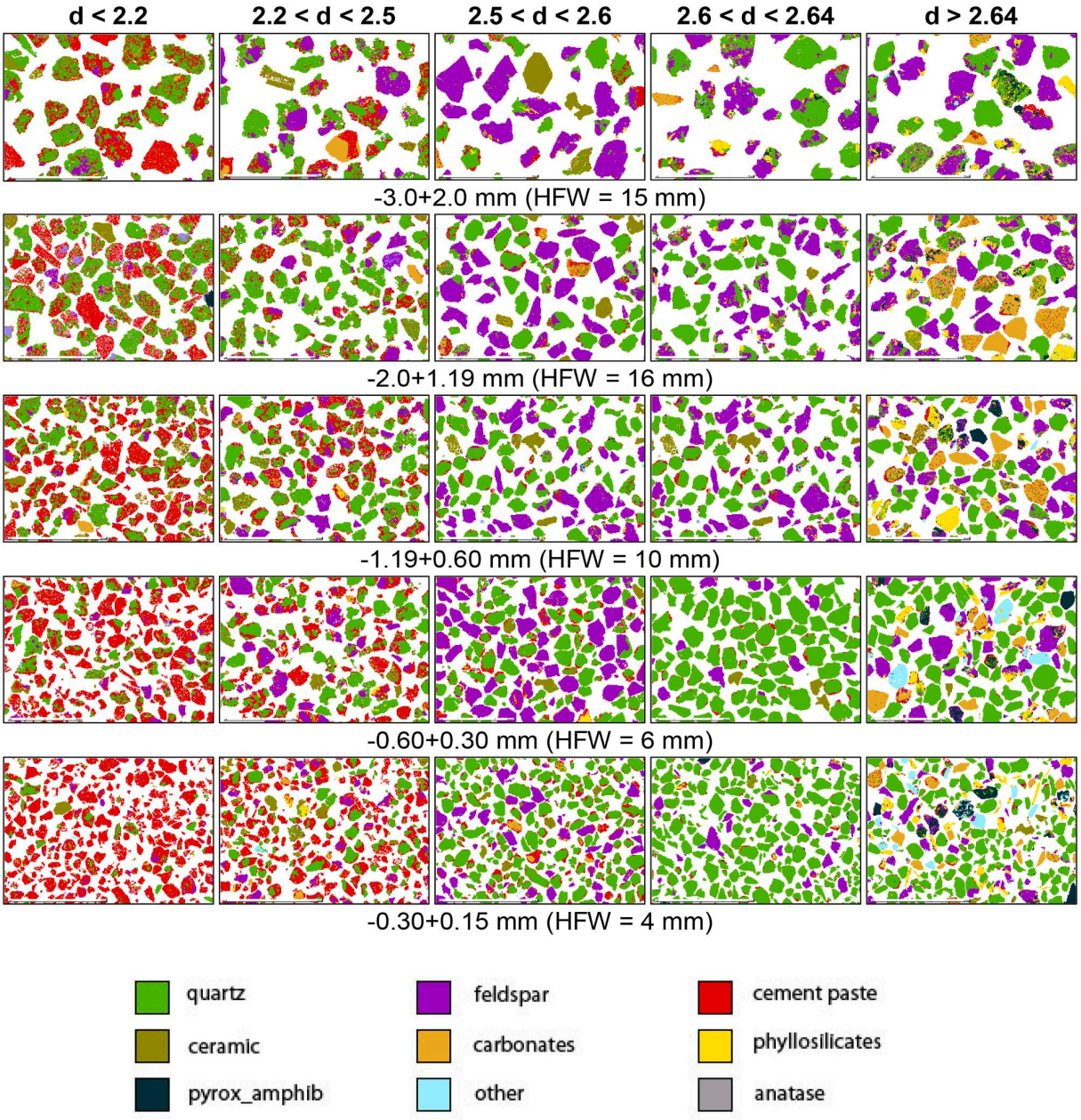

Fig. 6. Phase classification of particles in SEM-IA by size fraction and density products (HFW = horizontal field of view).

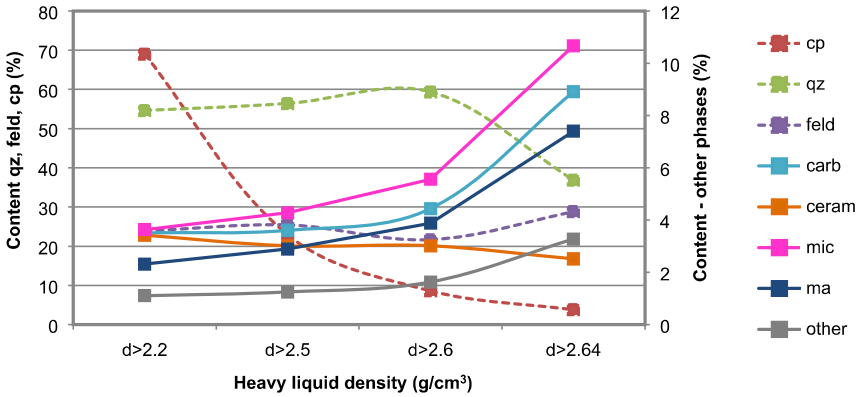

Fig. 7. Cumulative phase's content by density separation products (total 3.0–0.15 mm).

Table 3
Partition of Ca on bearing phases.

Fraction (mm)	Phases	Ca distribution (%)					Total by fraction
		<2.20	2.20–2.50	2.50–2.60	2.60–2.64	>2.64	
3.0–2.0	cp	94	86	75	36	12	60
	carb	5.7	14	25	46	51	27
	ma	-	-	-	12	31	11
2.0–1.2	cp	96	91	82	65	16	71
	carb	3.6	9.0	12	8.3	61	22
	ma	-	-	4.8	23	18	5.8
1.2–0.60	cp	97	92	90	73	11	75
	carb	3.1	6.9	10	13	59	17
	ma	-	-	-	12	24	5.6
0.60–0.30	cp	95	93	86	98	14	81
	carb	5.1	7.3	6.9	1.7	53	12
	ma	-	-	7.5	-	27	5.6
0.30–0.15	cp	95	93	76	98	19	93
	carb	4.5	7.4	12	1.9	49	5.2
	ma	-	-	12	-	25	1.7
Total 3.0–0.15	cp	**96**	**91**	**82**	**83**	**14**	77
	carb	4.3	8.9	13	8.4	**55**	16
	ma	-	-	5.7	6.8	**25**	5.6

Notes: cement paste (cp), carbonates (carb), mafic minerals (ma) – pyroxene + amphibole.

Table 4
Association of mineral phases by density and size fraction.

Sieve fraction (mm)	Mineral association	Products from heavy liquid separation (% mass)				
		<2.20	2.20–2.50	2.50–2.60	2.60–2.64	>2.64
3.0–2.0	free	12	34	74	94	96
	locked with CP	88	66	26	5,9	4,2
2.0–1.2	free	5,5	30	75	96	95
	locked with CP	95	70	25	4,0	5,3
1.2–0.60	free	8,7	23	72	95	95
	locked with CP	91	77	28	5,2	5,4
0.60–0.30	free	4,0	25	57	90	93
	locked with CP	96	75	43	10	7,4
0.30–0.15	free	6,6	11	50	89	90
	locked with CP	93	89	50	11	10

cp – cement paste.

The dense product at 2.60 g/cm^3 (Table 2, highlighted in green colour) present just 8.6% of the total cement paste in concentrate and 28.8% of the ceramics, while the yield of mineral phases would be higher than 60% in average, and reaches 95% in the case of mafic minerals. The results of phase's distribution clearly demonstrate that for each separation density, there is depletion on ceramics and cement paste recovery compared to the mass distribution, thus, there is enrichment on other mineral phases in the heavier concentrates.

Cement paste is dominant in the product density below 2.50 g/cm^3 (Table 2, highlighted in pink colour), which represents 77% of its total content in the sample for just 25.4% in mass. On the other hand, for the same product, the content of carbonates is minimum (from 2.5 to 3.2%) and mafic minerals are insignificant.

The composition of the product sink in 2.64 g/cm^3 is outstanding,

Table 5
Mineral liberation degree by sieve fraction for different proportions of phases in bearing particles.

Phases (% in area from the containing particle)	Liberation degree (%) by sieve fraction (mm)				
	3.00–2.00	2.00–1.20	1.20–0.60	0.60–0.30	0.30–0.15
≥ 50	99	98	98	98	97
≥ 80	92	90	90	93	91
≥ 90	82	80	82	85	82
≥ 95	74	75	75	76	70

since there is a remarkable increase in the content of carbonates and mafic minerals; 69% of the carbonates from the sample are concentrated in this product and 95% of the mafic minerals.

The content of each phase in cumulative products is exposed in Fig. 7; from this figure, it is possible to identify the content of cement paste (apart from the carbonates) for each separation density, as well as to any other phase. As an example, for a cement paste content lower than 10%, the separation density must be around 2.60 g/cm^3. The same interpretation can be used to any other phase, such as quartz, feldspar and other identified phases.

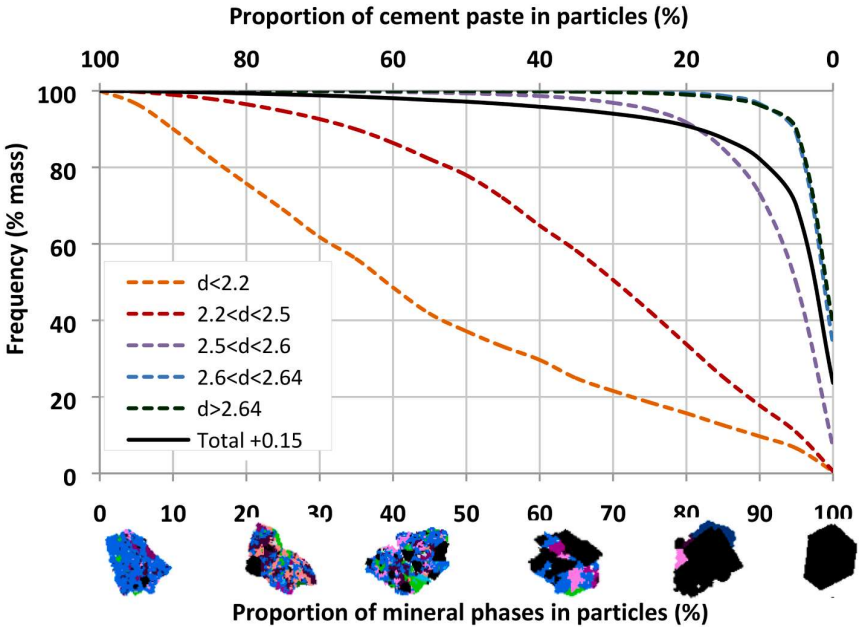

Fig. 8. Frequency of particles for different class of mineral particles by density separation products (total sample 3.00–0.15 mm).

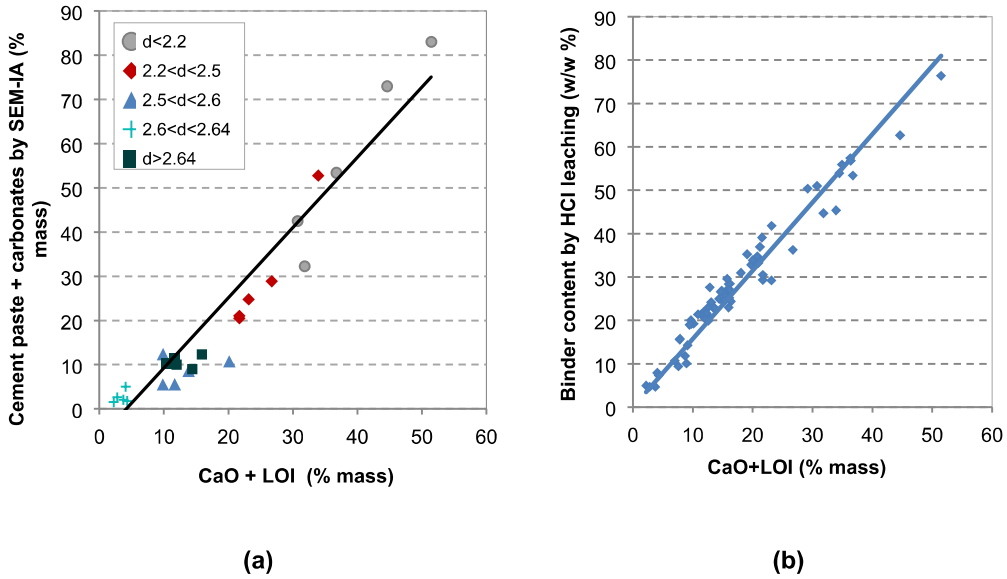

Fig. 9. Correlations between the content of cement paste and carbonates by SEM-IA, CaO + LOI and HCl leaching.

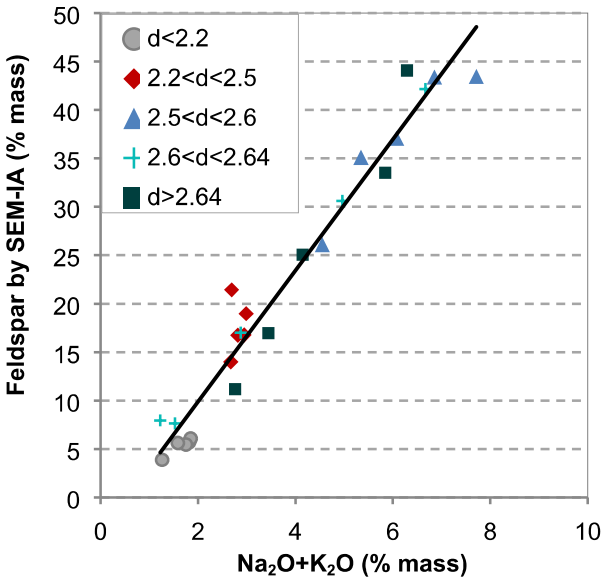

Fig. 10. Correlations between the content of feldspar by SEM-IA and chemical results.

3.2. Partition of Ca on bearing phases

Regarding the chemical composition, the partition of calcium (Ca) in the bearing phases is shown in Table 3 and indicates the proportion of this element that is associated with each phase.

For the whole sample characterized (total sample 3.0–0.15 mm), in products with density below 2.64 g/cm^3, the partition of Ca on bearing phases (Table 3) revealed that the calcium is essentially associated with the cement paste (>90% on average, varying from 82 to 96% – (Table 3) in blue colour). Nevertheless, on the products sink at 2.64 g/cm^3, just 14% of the calcium is associated with this phase due to the large presence of other calcium-bearing phases (calcite/dolomite/pyroxene/amphibole – (Table 3, in pink).

The Ca distribution in terms of particle size is more relevant on coarsest fractions since the content of carbonates, pyroxene/amphiboles are higher, and they account as Ca-bearing phases.

In conclusion, the higher the density of the product separation, the lower the content of cement paste, however the amount of Ca increases since it is associated with other phases. So, neither acid leaching nor the sum of CaO and LOI quantify correctly the amount of cement paste when limestone is present or other calcium-bearing phases.

3.3. Phases' association and liberation

The results of image analysis allow a detailed characterization of the associations of each phase, although for evaluating phase's liberation the results were coupled in just two major groups: a) cement paste, b) mineral phases (all other phases identified except cement paste, composed by quartz, feldspar, carbonates, ceramic and others). The occurrence of mineral phases into free[1] or locked[2] particles with cement paste is summarized in Table 4.

The mineral liberation curves by particle composition represented by the frequency of particles with different proportion of cement paste (0%, 5%, 10% … 90%,100%) are shown in Fig. 8, for the total sample (fraction 3.0–0.15 mm) by density products and the liberation degree by size fraction in Table 5.

There is a progressive increasing on the proportion of free particles (particles free of attached cement paste) on heavier products due to the phase's liberation (Table 4, Fig. 9).

For products float at 2.50 g/cm^3 (Table 3), most particles are locked with cement paste (from 88 to 96% for product <2.20 and 66 to 89% for product 2.20–2.50 g/cm^3); for product sink at 2.50 and float at 2.60 g/cm^3, the proportion of locked particles decrease to intermediate values (25 to 28% for fractions >0.60 mm and 43 to 50% on finer fractions). For products sink at 2.60, the proportion of locked particles decreases markedly and the proportion of free particles goes up to 96%, indicating that a density separation will lead to a heavy product with low content of cement paste and also a high proportion of pure mineral particles with no paste.

Taking into consideration the sieve fractions, it is noteworthy the decreasing on phase's liberation on fractions below 0.60 mm due to the intimate associations of fine particles of sand and cement paste that composes the mortar or concrete (Table 4, Fig. 9).

The liberation degree by sieve fraction is very similar and up to 95% of mineral phases by area. Particles containing <10% of cement paste in area (>90% of mineral phase) represent from 80 to 85% of the total particles; whilst if the aim is to attain particles with <5% of cement paste attached, the proportion of particles decrease to values between 70 and 76%. This is a remarkable data to drive recycling processing.

From Fig. 9, it is possible to establish the separation density in which the desired content of cement paste can be attained, i.e., for a particle containing at least 90% of mineral phases (maximum of 10% of cement paste), there will be achieve a sample mass recovery around 80% for the total sample fractions. If we analyse each density separation, it its remarkable that density below 2.50 g/cm^3 is enriched in particles associated to cement paste.

3.4. Phases quantification by SEM-IA and chemical analyses

The sum of the contents of cement paste and carbonates assessed by SEM-IA shows a linear correlation with the sum of CaO by XRF and LOI at 1,050 °C (Fig. 9a), which, in turn, presents a good correlation with the estimate of cement paste by acid leaching (Fig. 9b). It is important to highlight that both methods are not selective to cement paste but are correlated to the sum of carbonate and cement paste content. The chemical composition of all products is detailed in Table 6 – Appendix III.

It is noteworthy that this correlation considers the sum of carbonates and cement paste. In higher density products, the content of carbonates (calcite and dolomite) increases and the content of cement paste decreases to values under 2% (Table 2), so the estimation by chemical analysis is no longer accurate.

Thus, the estimation of the cement paste content by HCl leaching or by CaO + LOI in products with higher density becomes even more inaccurate, underestimating the quality of the recycled aggregates products (Fig. 9). The results are confirmed by analyzing the distribution of calcium in the cement paste by SEM-IA.

Moreover, the content of feldspar (Fig. 10.) is directly related to the sum of the Na_2O and K_2O assessed by XRF, thus by chemical analysis results it is possible to infer if the proportion of feldspar are increasing or decreasing.

4. Conclusions

The cement paste content, carbonates and other phases was precisely quantified by SEM-based automated image analysis in fine recycled aggregates, as well as their associations. Therefore, it is possible to evaluate the recycling processing efficiency and control the composition of the final product, as well as indicate the appropriate comminution size to attain better liberation degree (cement paste removal).

[1] Free particle indicates a particle composed by one single phase (>95% in area), i.e. it is not associated with cement paste in this specific study

[2] Locked particles are the ones composed by mineral phase plus cement paste

The results of image analysis allow a detailed characterization of the associations of each phase and demonstrated an increasing in the proportion of particles without cement paste attached in denser products, as expected. For products sink at 2.60 g/cm^3, the proportion of free particles goes up to 96%. Regarding particle size, it was demonstrated that particles >1.2 mm present an intrinsic association with porous phases and lower liberation degree. For fractions finer than 1.2 mm, the liberation degree increases dramatically, indicating that it is a better top size for grinding.

At high density products (d >2.64 g/cm^3), just 14% of the total calcium is associated with cement paste (fraction 3.0–0.15 mm) and 80% associated to calcite, dolomite, pyroxenes and amphiboles, the remaining 6% is associate at the fines (<0.5 mm). The cement paste evaluation by simple methods such as loss on ignition plus CaO and acid leaching tests cannot be applied correctly when limestone is present as aggregate. Highers the content of carbonate less representative is the tested simple methods for cement paste quantification.

The correlations between the sum of CaO and LOI and cement paste + carbonates, as well as comparison to the cement plus carbonate content estimated by acid leaching, demonstrate the reliability SEM-based image analysis to quantify the cement paste in fine recycled aggregates.

Declaration of Competing Interest

The authors declare that they have no known competing financial interests or personal relationships that could have appeared to influence the work reported in this paper.

Acknowledgments

The authors gratefully acknowledge the following funding agencies: CAPES project 88881 068109 2014-01, FAPESP process 2009/54007-0 and 2016/01456-6, CNPq project 478142/2009-9 and 550437/2010-0; and the infrastructure provided by the Technological Characterization Laboratory (LCT-USP) at the University of São Paulo. The information and views set out in this study are those of the authors and do not necessarily reflect the opinions of the funding agencies. The authors also thank the geologist Rafael Ribeiro de Franca for his work.

Appendix I

Schema for the calculation of the liberation degree

$$Liberation\ degree = \frac{Phase\ of\ interest\ (free)}{Total\ of\ phase\ of\ interest\ (free+locked)} \times 100.$$ Fig. 11.

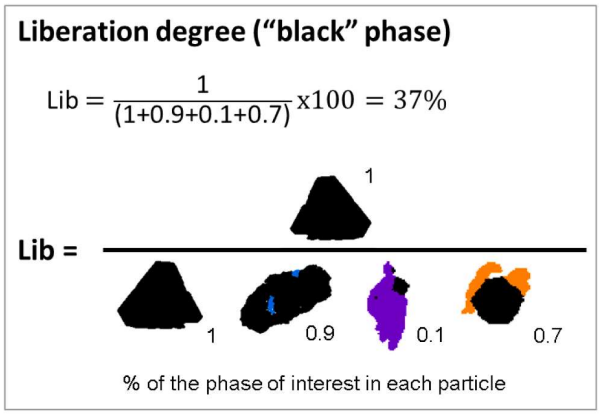

(a) Liberation degree of the "black" phase

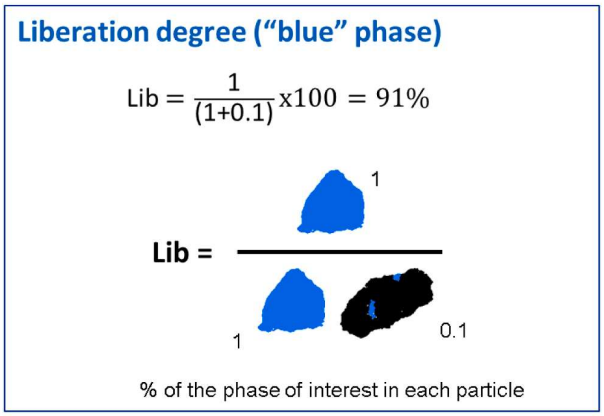

(b) Liberation degree of the "blue" phase

Fig. 11. Examples for the calculation of the liberation degree for different phases from a sample; (a – "black" phase; b – "blue" phase).

Appendix II

Brief description of SEM–IA analysis

The SEM-based image analysis system used (MLA system) consists of a software that controls energy dispersive spectrometer (EDS) and scanning electron microscope (SEM) detectors, automatically acquiring X-ray EDS images and spectra. Typically, around 40 to 100 images/frames (containing 4,000 to 20,000 particles) are acquired for each polished section/sample. Subsequently, an off-line processing of the images of the particles and respective X-ray data generates digital maps of the minerals and the proportions in mass, mineral associations and degree of release, among other parameters, are calculated.

MLA can combine electron backscattered (BSE) image and characteristic X-ray spectra. The use of BSE images for grain analysis has the advantage of having a substantially higher resolution than that obtained by X-rays, around a few tens of nanometers (depending on the equipment and magnification) versus a few micrometers, in addition to being much faster.

There are various ways of collecting the MLA data, which are used in different types of materials depending on the purpose of the study and the characteristics of the samples. The most commonly used measurement modes are described below, with the GXMAP mode being applied in this study:

1. *Standard BSE release analysis (BSE):* is the most basic measurement mode of MLA release analysis, where a series of images are collected online and then processed offline to produce release data. This measurement mode is based only on the different shades of gray in the BSE image.
2. *Extended BSE liberation analysis (XBSE):* In this measurement mode each BSE image is collected and segmented to delineate mineral grain contours and then each mineral grain is analysed by only one X-ray spotted in the centroid of the grain.
3. *Ford analysis or grain-based X-ray mapping (GXMAP):* this is a selective mapping method. Employs X-ray mapping according to a grid of dots for phases that cannot be segmented by different shades of gray in the BSE image. The operator selects the grains to be mapped by means of an interval in the histogram of the BSE image or by a certain X-ray spectrum.
4. *Sparse phase liberation analysis* (SPL): this measurement mode searches for BSE images with particles containing the phase of interest, using for this the grayscale range of the phase of interest; it then performs an XBSE analysis on the particle.
5. *X-ray modal analysis (XMOD):* This measurement mode only produces modal mineralogy data. In this method, a grid of points is defined by the operator and for each grid point (on the particles) a ray spectrum is collected. The XMOD method can also be implemented for the linescan mode, which produces data from the traditional linear intercept measurement mode (point spacing in the "x" direction is 1 pixel). In this method, the BSE image is used only to differentiate the background particles (resin). Fig. 12.

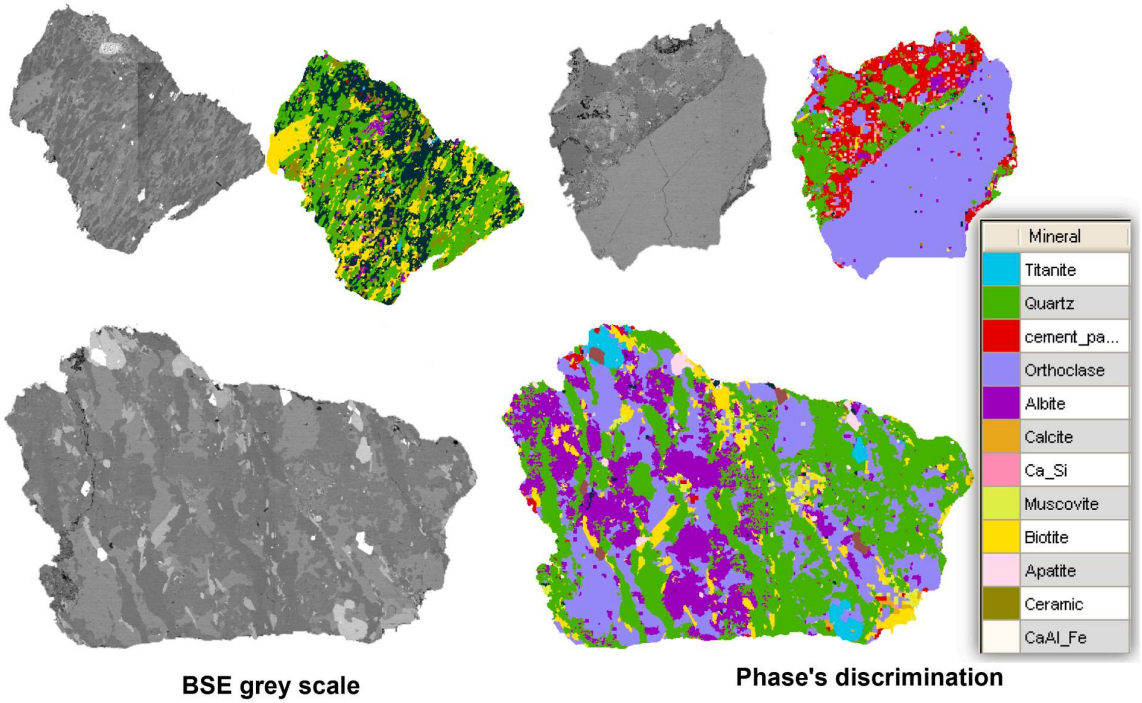

Fig. 12. Phases' discrimination of complex texture particles by the adopted procedure.

Appendix III

Products composition by size and density

Figs. 13-15 and Table 6.

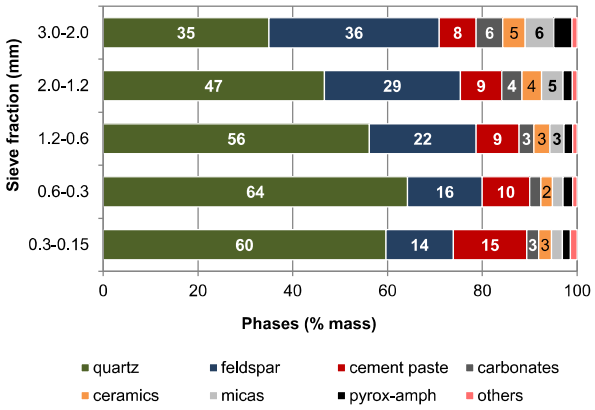

Fig. 13. Products composition by sieve fraction.

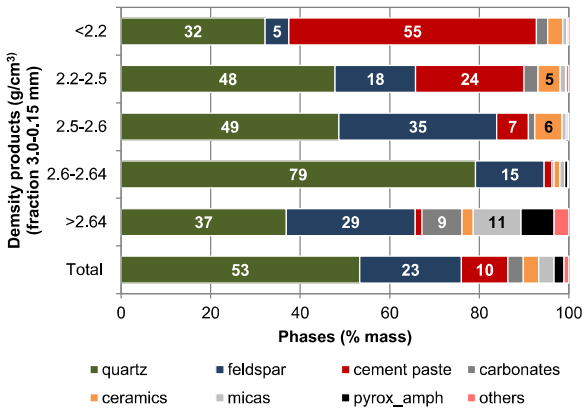

Fig. 14. Products composition by density (total 3.0-0.15 mm).

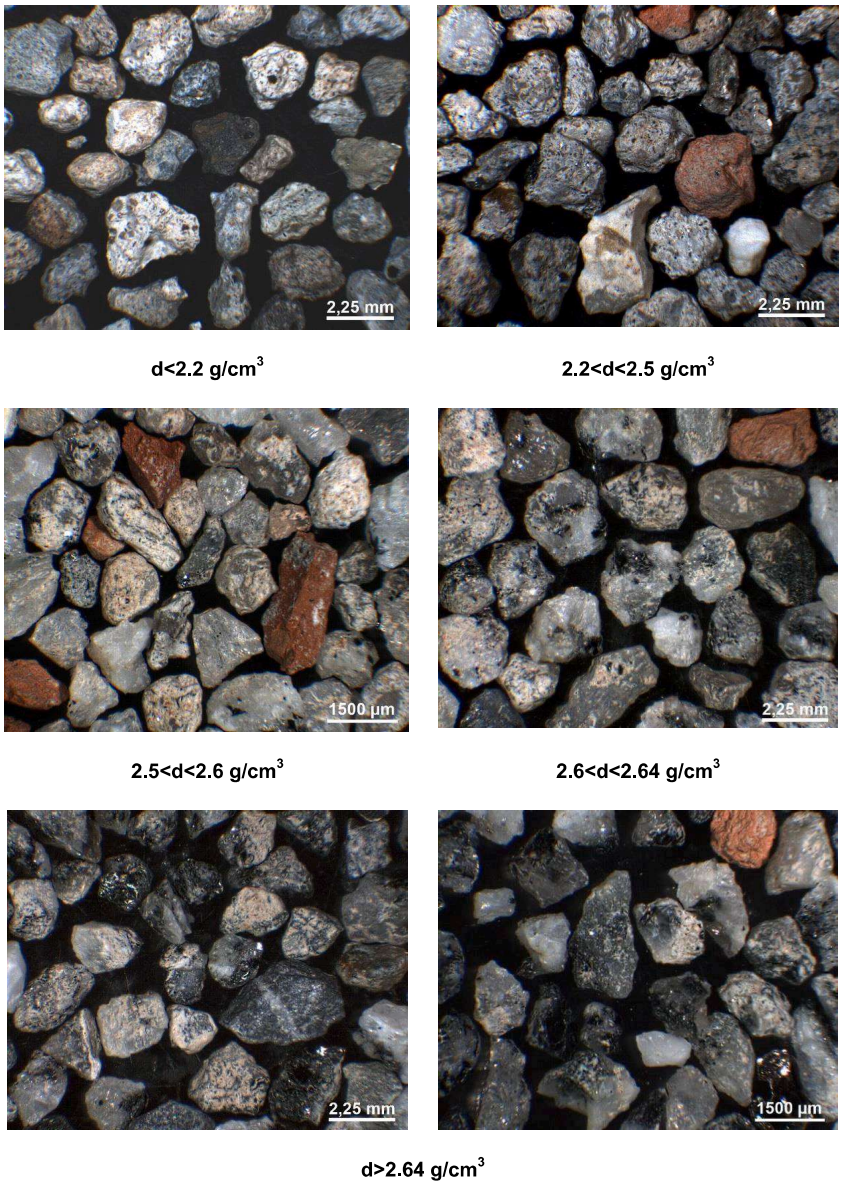

Fig. 15. Images of products from heavy liquid separation products illustrating the composition attained by SEM-IA.

Table 6
Chemical composition of each product (by density and size fraction).

Products (size/density)	Content (% mass)								
	SiO_2	Al_2O_3	Fe_2O_3	CaO	LOI	Na_2O	K_2O	MgO	Binder-HCl
−3.0 + 2.0 mm d < 2.2	52.1	6.67	3.20	18.9	12.9	0.49	1.33	1.94	44.7
−3.0 + 2.0 mm 2.2 < d < 2.5	62.3	6.71	3.00	12.9	8.83	0.65	2.04	1.48	29.3
−3.0 + 2.0 mm 2.5 < d < 2.6	64.2	13.2	3.07	5.07	3.65	2.31	5.40	0.88	11.8
−3.0 + 2.0 mm 2.60 < d < 2.64	71.1	11.8	3.91	2.90	1.17	3.03	3.64	0.55	7.90
−3.0 + 2.0 mm d > 2.64	55.6	13.4	5.72	9.12	5.27	3.26	3.03	2.38	26.6
−2.0 + 1.19 mm d < 2.2	52.3	6.73	2.58	18.3	12.4	0.52	1.33	1.90	51.0
−2.0 + 1.19 mm 2.2 < d < 2.5	62.4	6.78	2.59	12.7	8.96	0.59	2.23	1.49	30.5
−2.0 + 1.19 mm 2.5 < d < 2.6	67.6	12.0	2.46	4.19	3.41	1.81	5.05	0.76	9.40
−2.0 + 1.19 mm 2.60 < d < 2.64	76.4	9.20	2.39	2.06	2.27	2.35	2.61	0.38	7.29
−2.0 + 1.19 mm d > 2.64	54.9	12.9	5.47	9.30	6.59	3.06	2.79	2.35	25.7
−1.19 + 0.60 mm d < 2.2	46.4	7.22	2.47	21.6	15.1	0.42	1.34	2.03	53.4
−1.19 + 0.60 mm 2.2 < d < 2.5	60.9	7.01	2.31	13.3	9.80	0.58	2.41	1.46	29.2
−1.19 + 0.60 mm 2.5 < d < 2.6	71.4	9.31	3.30	4.00	3.00	1.26	4.09	0.57	10.7

(*continued on next page*)

Table 6 (*continued*)

Products (size/density)	Content (% mass)								
	SiO_2	Al_2O_3	Fe_2O_3	CaO	LOI	Na_2O	K_2O	MgO	Binder-HCl
−1.19 + 0.60 mm 2.60 < d < 2.64	84.7	5.60	2.68	1.65	0.57	1.39	1.49	0.21	4.97
−1.19 + 0.60 mm d > 2.64	63.2	9.87	6.06	7.13	4.82	2.09	2.06	1.88	19.1
−0.60 + 0.30 mm d < 2.2	40.6	7.70	2.97	25.3	19.3	0.36	1.23	2.38	62.7
−0.60 + 0.30 mm 2.2 < d < 2.5	55.9	7.26	2.47	15.1	11.7	0.53	2.42	1.68	36.3
−0.60 + 0.30 mm 2.5 < d < 2.6	70.2	9.73	2.03	4.82	4.31	1.04	5.03	0.58	14.2
−0.60 + 0.30 mm 2.60 < d < 2.64	88.1	3.51	2.02	1.74	2.00	0.84	0.69	0.19	4.67
−0.60 + 0.30 mm d > 2.64	65.2	9.09	6.61	6.66	4.95	1.50	1.94	2.04	22.5
−0.30 + 0.15 mm d < 2.2	32.2	8.27	3.24	30.6	20.9	0.32	0.95	3.15	76.4
−0.30 + 0.15 mm 2.2 < d < 2.5	49.3	8.11	2.77	18.8	15.2	0.50	2.17	2.26	45.4
−0.30 + 0.15 mm 2.5 < d < 2.6	74.1	7.83	1.82	4.68	4.28	0.88	3.67	0.51	10.1
−0.30 + 0.15 mm 2.60 < d < 2.64	90.4	2.99	1.47	1.66	1.13	0.75	0.47	0.15	4.67
−0.30 + 0.15 mm d > 2.64	67.1	7.76	6.45	5.95	4.50	1.03	1.73	1.96	17.9
Total −3.0 + 0.15 mm d < 2.2	44.2	7.36	2.89	23.3	16.2	0.42	1.22	2.32	58.5
Total −3.0 + 0.15 mm 2.2 < d < 2.5	59.2	7.08	2.59	14.1	10.4	0.58	2.26	1.61	32.7
Total −3.0 + 0.15 mm 2.5 < d < 2.6	70.4	9.90	2.49	4.51	3.75	1.34	4.45	0.63	11.0
Total −3.0 + 0.15 mm 2.60 < d < 2.64	85.1	5.19	2.22	1.82	1.40	1.30	1.28	0.23	5.30
Total −3.0 + 0.15 mm d > 2.64	60.3	11.0	5.97	7.87	5.27	2.37	2.41	2.14	22.7

References

[1] C.P. Ginga, J.M.C. Ongpeng, M.K.M. Daly, Circular economy on construction and demolition waste: A literature review on material recovery and production, Materials. 13 (2020) 1–18, https://doi.org/10.3390/ma13132970.

[2] P. Ghisellini, M. Ripa, S. Ulgiati, Exploring environmental and economic costs and benefits of a circular economy approach to the construction and demolition sector, A literature review, Journal of Cleaner Production. 178 (2018) 618–643, https://doi.org/10.1016/j.jclepro.2017.11.207.

[3] M.S. de Juan, P.A. Gutiérrez, Study on the influence of attached mortar content on the properties of recycled concrete aggregate, Constr. Build. Mater. 23 (2) (2009) 872–877, https://doi.org/10.1016/j.conbuildmat.2008.04.012.

[4] H. Ogawa, T. Nawa, Improving the Quality of Recycled Fine Aggregate by Selective Removal of Brittle Defects, J. Adv. Concr. Technol. 10 (12) (2012) 395–410, https://doi.org/10.3151/jact.10.395.

[5] F. Tomosawa, T. Noguchi, M. Tamura, The way concrete recycling should be, Journal of Advanced, Technology. 3 (2005) 3–16.

[6] C. Ulsen, H. Kahn, G. Hawlitschek, E.A. Masini, S.C. Angulo, Separability studies of construction and demolition waste recycled sand, Waste Manage. 33 (3) (2013) 656–662, https://doi.org/10.1016/j.wasman.2012.06.018.

[7] C. Ulsen, E. Tseng, S.C. Angulo, M. Landmann, R. Contessotto, J.T. Balbo, H. Kahn, Concrete aggregates properties crushed by jaw and impact secondary crushing, J. Mater. Res. Technol. 8 (1) (2019) 494–502, https://doi.org/10.1016/j.jmrt.2018.04.008.

[8] J.I. Alvarez, A. Martín, P.J. García Casado, I. Navarro, A. Zornoza, Methodology and validation of a hot hydrochloric acid attack for the characterization of ancient mortars, Cem. Concr. Res. 29 (7) (1999) 1061–1065, https://doi.org/10.1016/S0008-8846(99)00090-3.

[9] S.C. Angulo, A. Mueller, Chemical-mineralogical characterization of C&D waste recycled aggregates from São Paulo, Brazil, Constructions. 42 (2009) 739–748, https://doi.org/10.1016/j.wasman.2008.07.009.

[10] Z. Zhao, S. Remond, D. Damidot, W. Xu, Influence of hardened cement paste content on the water absorption of fine recycled concrete aggregates, Journal of Sustainable Cement-Based Materials. 2 (3-4) (2013) 186–203, https://doi.org/10.1080/21650373.2013.812942.

[11] S. Macedo, C. Ulsen, A. Mueller, Quantification of residual cement paste on recycled concrete aggregates containing limestone by selective dissolution, Constr. Build. Mater. 229 (2019), 116875, https://doi.org/10.1016/j.conbuildmat.2019.116875.

[12] M.P. Jones, Applied Mineralogy – A Quantitative Approach, 1a Edição, Graham and Trotman Ltd., Assinipi Park, 1987.

[13] W. Petruk, Applied Mineralogy in the Mining Industry, 1st ed., Elsevier Science, 2000.

[14] R.O. Burt, Gravity Concentration Technology, Elsevier, Amsterdam, 1984.

[15] E.C. Kelly, J. Spottiswood, Introduction to Mineral Processing, John Willey, New York, 1982.

[16] L. Evangelista, J. de Brito, Concrete with fine recycled aggregates: A review, European Journal of Environmental and Civil, Engineering. 18 (2) (2014) 129–172, https://doi.org/10.1080/19648189.2013.851038.

[17] R. Fandrich, Y. Gu, D. Burrows, K. Moeller, Modern SEM-based mineral liberation analysis, Int. J. Miner. Process. 84 (1-4) (2007) 310–320, https://doi.org/10.1016/j.minpro.2006.07.018.

[18] M.P. Jones, Applied Mineralogy – A Quantitative Approach, Graham & Trotman, United States, 1987.

[19] D.N. Sutherland, P. Gottlieb, Application of Automated Quantitative Mineralogy in Mineral Processing, Miner. Eng. 4 (7-11) (1991) 753–762.

[20] Y. Gu, Automated scanning electron microscope based mineral liberation analysis, Journal of Minerals and Materials Characterization and Engineering. 2 (2003) 33–41, https://doi.org/10.4236/jmmce.2003.21003.

[21] A. Abbas, G. Fathifazl, B. Fournier, O.B. Isgor, R. Zavadil, A.G. Razaqpur, S. Foo, Quantification of the residual mortar content in recycled concrete aggregates by image analysis, Mater. Charact. 60 (7) (2009) 716–728, https://doi.org/10.1016/j.matchar.2009.01.010.

[22] S. Pradhan, S. Kumar, S. v. Barai, Multi-scale characterisation of recycled aggregate concrete and prediction of its performance, Cement and Concrete Composites. 106 (2020) 103480. 10.1016/j.cemconcomp.2019.103480.

[23] Z. Zhao, S. Remond, D. Damidot, W. Xu, Influence of fine recycled concrete aggregates on the properties of mortars, Constr. Build. Mater. 81 (2015) 179–186, https://doi.org/10.1016/j.conbuildmat.2015.02.037.

[24] Y. Kim, A. Hanif, M. Usman, W. Park, Influence of bonded mortar of recycled concrete aggregates on interfacial characteristics – Porosity assessment based on pore segmentation from backscattered electron image analysis, Constr. Build. Mater. 212 (2019) 149–163, https://doi.org/10.1016/j.conbuildmat.2019.03.265.

[25] L. Evangelista, M. Guedes, J. de Brito, A.C. Ferro, M.F. Pereira, Physical, chemical and mineralogical properties of fine recycled aggregates made from concrete waste, Constr. Build. Mater. 86 (2015) 178–188, https://doi.org/10.1016/j.conbuildmat.2015.03.112.

[26] G. Barbery, Mineral Liberation: Measurement, Simulation and Practical use in Mineral Processing, Les Editions GB, Pennsylvania, 1991.

[27] E.E. Underwood, Quantitative Stereology, Addison-Wesley Pub. Co, 1970.

[28] A.M. Gaudin, Principles of Mineral Dressing, MacGraw-Hill, New York, 1932.

[29] C. Ulsen, H. Kahn, G. Hawlitschek, E.A. Masini, S.C. Angulo, V.M. John, Production of recycled sand from construction and demolition waste, Constr. Build. Mater. 40 (2013) 1168–1173, https://doi.org/10.1016/j.conbuildmat.2012.02.004.

[30] C. Ulsen, J.L. Antoniassi, I.M. Martins, H. Kahn, High quality recycled sand from mixed CDW – Is that possible? J. Mater. Res. Technol. 12 (2021) 29–42, https://doi.org/10.1016/j.jmrt.2021.02.057.

[31] J. Tomas, M. Schreier, T. Groger, Liberation and separation of valuables from building material waste, Rewas'99 Global Symposium on Recycling, Waste Treatment and Clean Technology Volume I-Iii. (1999) 461–470.

[32] Magnus Bengtsson, C. Magnus Evertsson, Measuring characteristics of aggregate material from vertical shaft impact crushers, Miner. Eng. 19 (15) (2006) 1479–1486, https://doi.org/10.1016/j.mineng.2006.08.003.

[33] Mats Lindqvist, Energy considerations in compressive and impact crushing of rock, Miner. Eng. 21 (9) (2008) 631–641, https://doi.org/10.1016/j.mineng.2007.11.013.

[34] V.A. Quarcioni, M.A. Cincotto, Optimization of calculation method for determination of composition of hardened mortars of Portland cement and hydrated lime made in laboratory, Constr. Build. Mater. 20 (2006) 1069–1078.

[35] L. v. d. Plas, A.C. Tobi, A chart for judging the reliability of point counting results, American Journal of Science. 263 (1965) 722–724. 10.2475/ajs.263.8.722.